Mice With A Cleavage-Resistant N-Cadherin Exhibit Synapse Anomaly in the Hippocampus and Outperformance in Spatial Memory Tasks

Megumi Asada-Utsugi
Kyoto University Graduate School of Medicine
Kengo Uemura
Kyoto University Graduate School of Medicine
Masakazu Kubota
Osaka Medical College
Yasuha Noda
Kyoto University Graduate School of Medicine
Yasutaka Tashiro
Kyoto University Graduate School of Medicine
Maiko T Uemura
Kyoto University Graduate School of Medicine
Hodaka Yamakado
Kyoto University Graduate School of Medicine
Makoto Urushitani
Shiga Medical University
Ryosuke Takahashi
Kyoto University Graduate School of Medicine
Satoko Hattori
Fujita Health University
Tsuyoshi Miyakawa
Fujita Health University
Natsumi Ageta-Ishihara
Nagoya University
Katsunori Kobayashi
Nippon Medical School
Makoto Kinoshita
Nagoya University
Ayae Kinoshita (kinoshita.ayae.6v@kyoto-u.ac.jp)
Kyoto University Graduate school of medicine

Research

Keywords: N-cadherin, ADAM10, synapse, hippocampus, working memory

Posted Date: August 31st, 2020

DOI: https://doi.org/10.21203/rs.3.rs-64344/v1

Version of Record: A version of this preprint was published on January 25th, 2021. See the published version at https://doi.org/10.1186/s13041-021-00738-1.

Abstract

N-cadherin is a homophilic cell adhesion molecule that stabilizes excitatory synapses, by connecting pre- and post-synaptic termini. Upon NMDA receptor (NMDAR) activation by glutamate, membrane-proximal domains of N-cadherin are cleaved serially by a-disintegrin-and-metalloprotease 10 (ADAM10) and then presenilin 1(PS1, catalytic subunit of the γ-secretase complex). To assess the physiological significance of the initial N-cadherin cleavage, we engineer the mouse genome to create a knock-in allele with tandem missense mutations in the mouse N-cadherin/Cadherin-2 gene (*Cdh2* $^{R714G, I715D}$, or GD) that confers resistance to proteolysis by ADAM10 (GD mice). GD mice showed a better performance in the radial maze test, with significantly less revisiting errors after intervals of 30 and 300 sec than WT and a tendency for enhanced freezing in fear conditioning. Interestingly, GD mice reveal higher complexity in the tufts of thorny excrescence in the CA3 region of the hippocampus. Fine morphometry with serial section transmission electron microscopy (ssTEM) and three-dimensional (3D) reconstruction reveals significantly higher synaptic density, significantly smaller PSD area, and normal dendritic spine volume in GD mice. This knock-in mouse has provided *in vivo* evidence that ADAM10-mediated cleavage is a critical step in N-cadherin shedding and degradation and involved in the structure and function of glutamatergic synapses, which affect the memory function.

Introduction

N-cadherin is a key cell adhesion molecule required not only for dendrite arborization and axon guidance during development, but also for post-developmental generation, maintenance, and remodeling of synapses [1,2,3,4,5,6]. N-cadherin abounds in active zones of immature synapses, and at the periphery of mature synapses [7], indicating that N-cadherin changes its location as well as its functional role between synaptogenesis and mature synapses. Transsynaptic contact mediated by the N-cadherin/catenin complex is a determinant of neuro-transmission and spine morphology, and reciprocally, synaptic activity modulates the expression, conformation, targeting, degradation and proteolytic cleavage of N-cadherin [8,9,10,11,12,13].

As with other synaptic adhesion molecules, activity-dependent and -independent proteolytic cleavage of surface-presented N-cadherin attenuates transsynaptic adhesive force, which facilitates synaptic remodeling [14,15,16]. A representative case is ADAM10-meditated cleavage at post-developmental excitatory synapses, followed by PS1/gamma-secretase-mediated (epsilon) cleavage, which releases a nuclear-targeting fragment CTF2 from N-cadherin [17,18,19].

Inhibition of the ADAM10-meditated initial cleavage increases the steady-state level of the full-length N-cadherin. Notably, stabilization of N-cadherin by inhibition of ADAM10 activity increases the spine head volume and the recruitment of GluR1into the postsynaptic compartment, thereby regulating function of AMPA receptors at the hippocampal excitarory synapses. (28) However, most of these findings are based on pharmacological experiments with cultured neurons or brain slices, and *in vivo* relevance had never been tested. (28) Thus, we set up to test the impact of ADAM10-mediated N-cadherin cleavage on animal

behavior. To analyze this, on the basis of our previous studies [20], we created a line of knock-in mice that express N-cadherin with a mutation resistant to ADAM10-mediated cleavage (GD mice).

Here, we demonstrate that the GD mice show higher fidelity in a working memory-dependent task than WT mice in the radial maze test. In the fear conditioning test, GD mice show a tendency for enhanced freezing. This behavioral change is accompanied by higher complexity in the tufts of thorny excrescence and significantly higher synaptic density, significantly smaller PSD area, and normal dendritic spine volume in the CA3 region of the hippocampus. Our mouse model helps address the open questions as to the physiological and pathological impacts of the cleavage-defective N-cadherin on synapse morphology and transmission, learning and memory, and other brain functions.

Results

Generation of a knock-in allele encoding the ADAM10-resistant mutant of N-cadherin

Our previous *in vitro* analysis showed that a tandem substitution mutation near the transmembrane domain of mouse N-cadherin (R714G/I715D, hereafter GD; Fig. 1A) confers resistance to ADAM10 [20]. To assess the physiological significance of ADAM10-mediated cleavage of N-cadherin in the brain, we designed a targeting vector to replace exon 13 of the mouse *Cdh2* gene with the GD mutant exon, by homologous recombination (Fig. 1A). After gene targeting of an ES cell line (Bruce4) derived from C57BL/6J strain, we screened Neomycin-resistant clones for a GD allele ($Cdh2^{R714G,\ I715D}$) by southern blotting, PCR, and sequencing of the genomic DNA (data not shown). Chimeric mice generated through blastocyst injection of one of Cdh2R714G, I 715D/+ ES cell clones into C57BL/6J embryos were bred with WT mice to yield heterozygous (Cdh2R714G, I715D/+) mice with the genetic background of C57BL/6J. The floxed Neomycin-resistant gene cassette was removed by breeding with CAG-Cre driver C57BL/6J mice. After confirming mendelian inheritance of the GD allele, we consistently compared homozygous GD mutant ($Cdh2^{R714G,\ I715D/R714G,\ I715D}$) and WT ($Cdh2^{+/+}$) male littermates born from heterozygous parents.

A mutant N-cadherin that is uncleavable by ADAM10 is relatively stable on the cell surface

First, to assess the resistance of GD mutant cadherin to ADAM10-mediated cleavage, we expressed wildtype (WT) or GD mutant N-cadherins, each tagged with HA epitope, in CHO cells. Their distribution patterns to the endoplasmic reticulum (ER), Golgi apparatus, and plasma membrane were largely comparable (Fig. 1B). On the other hand, surface biotinylation pulse-labeling followed by serial immunoblot assay for the HA epitope revealed that the cell surface fraction of GD N-cadherin was significantly higher than that of WT, indicative of a longer half-life (~ 12 h vs. ~4 h; Fig. 2A, B). These *in vitro* data indicate that GD mutation prolongs the retention of the full-length N-cadherin on the plasma membrane, indicating that ADAM-10 mediated cleavage of N-cadherin affects the level of cell-surface N-cadherin.

GD mutation does not show obvious difference in the content of major synapse proteins in synaptosome

Previous reports demonstrated that systemic and brain-selective null mutant mice of N-cadherin respectively exhibit severe systemic and neural anomalies [2,4,22], indicating a requirement of N-cadherin for development. In contrast, GD mice grow and breed normally, suggesting that the perturbation of the N-cadherin cleavage at the site does not cause obvious defects in embryonic and post-natal development.

Since cleaved ectodomain fragments of N-cadherin were barely detectable from the brain tissue samples, we examined the cytoplasmic fragment CTF1 in primary cultured cerebrocortical neurons and synaptosomal fractions from WT and GD mice. An antibody directed against the carboxyl terminus of N-cadherin detected native full-length N-cadherin and CTF1 in WT neurons, while CTF1 was not detected in GD neurons (Fig. 3B). CTF2, a g-secretase-mediated cleavage product of CTF1, was barely visible in this setting due to proteosomal degradation [20]. These data indicate the ADAM10-mediated cleavage-resistance of N-cadherin$^{R714G, I715D}$ *in vivo*, in line with the enhanced stability of exogenously expressed N-cadherin$^{R714G, I715D}$ in the surface bio-tinylation assay (Fig. 2A, B) and previous *in vitro* studies [20,21].

Next, we asked whether the content of excitatory synapse-related proteins is altered in the total brain lysate and the synaptosomal fraction of the GD mice. Immunoblot showed no obvious difference between steady-state levels of full length N-cadherins (GD and WT), and as to most of major post/pre/peri-synaptic proteins and activity-regulated proteins in those mice; *i.e.*, ADAM-10, PS1, GluA1, GluA2, AKT, phospho-AKT, syntaxin 6, synaptophysin, and GLT-1 in synaptosome. (Fig. 3A).

Behavioral profile of GD mice is largely normal, except for correct responses in a spatial working memory task

Next, we asked whether the insertion of GD mutation alter mouse behavior. As a means of unbiased functional screening for possible alterations in the GD mouse brain, we systematically conducted a learning memory test at 4 months of age. Male GD and WT littermates (n = 12, 9) were comparable in most of the physical and behavioral indices measured, but significantly differed in hippocampus-dependent tests and body weight, as follows (Supplemental Fig. S1–S4).

GD mice exhibited an unexpected phenotype in a spatial working memory task using 8-arm radial maze (Fig. 4A-G): The time spent for the acquisition of the reward from the opening of the gates was significantly longer in GD mice (Fig. 4C, G). Intriguingly, however, the revisiting errors after intervals of 30 and 300 secs were significantly less in GD mice than in WT (Fig. 4E, F), indicating that GD mice execute a working memory-dependent task with higher fidelity than WT mice. A similar trend, albeit statistically insignificant, was observed consistently in the probe test of the Barnes maze test, where GD mice tended to reduce the latency to find the escape hole and the number of errors made (Suppl. Figure 3).

In the fear conditioning test, GD mice showed a tendency for enhanced freezing (an index of associative memory) in the late phases of fear memory acquisition on Day 1 (Fig. 5A, B, left) and of re-exposure to the shock box (without tone cue or foot shock) on Day 2 (Fig. 5A, B, middle). Interestingly, in the cued

testing in altered context on Day 2, mutants showed enhanced freezing even before CS (Fig. 5A, B, right), indicating GD mice carried over learned behavior (freezing) the to a different context. Thus, this aberrant behavior could be interpreted as 'generalization'. Both wild-type and mutant mice reacted to unconditioned stimuli, although the time course of reaction was slightly different (Fig. 5C).

Hippocampal CA3 pyramidal neurons in GD mice develop anomalous synapses

To explore histological anomalies responsible for the behavioral alterations in GD mice, we conducted morphological analysis. The total weight and macroscopic architecture of the brain are normal in homozygous GD mice (Suppl. Figure 4). Given the abundance of *Cdh2* mRNA in the hippocampus, the highest in the CA3 pyramidal neurons, followed by the dentate gyrus granule cells (http://mouse.brain-map.org/experiment/show/79632275), we first examined the large specialized synapses between them. Golgi stain of the stratum lucidum of the CA3 region revealed significantly higher complexity in the tufts of thorny excrescence (Fig. 6A), which receive mossy fiber inputs from the granule cells. Statistical analysis revealed that thorny excrescence area (Fig. 6B) and tuft counts (Fig. 6C) were significantly increased in dendrites of GD mice.

Then, we focused on the synapses formed between associational/commissural fibers and pyramidal neurons in the stratum radiatum of the CA3 region to conduct serial section transmission electron microscopy (ssTEM) for 3D morphometry (Fig. 7). The density of asymmetrical (mostly glutamatergic) synapses measured using the dissector method was significantly higher in GD mice than WT mice (Fig. 7A: median value, 7 vs. 4, $p = 0.00062$, Mann-Whitney U test). The dendritic spine volume was comparable (Fig. 7B: median value, 0.015 vs. 0.015, $p = 0.23$, Mann-Whitney U test), whereas PSD area was significantly smaller in GD mice (Fig. 7C, D: median value, 0.030 vs. 0.035, $p = 0.0071$, Mann-Whitney U test). These findings, along with the Golgi stain results, indicate anomalies in synaptogenesis and/or remodeling of at least three types of synapses into CA3 pyramidal neurons of GD mice.

The associational/commissural fiber-pyramidal neuron synapses in CA3 exhibit marginal transmission anomalies

To explore possible functional alterations in the synapses formed between associational/commissural (A/C) fibers and pyramidal neurons in the stratum radiatum of the CA3 region, we conducted electrophysiological recording of field excitatory postsynaptic potentials (EPSPs), using acute hippocampal slices from GD and WT mice. Indices of basal synaptic transmission (*i.e.*, fiber volley amplitude, field EPSP slope, and paired-pulse facilitation) were largely comparable between GD and WT slices (Fig. 8A-C). However, the dependence of the synaptic response on the stimulus intensity was altered, with a trend of reduced EPSP slopes at higher stimulus intensities in GD mice (Fig. 8B). While high-frequency stimulation induced stable long-term potentiation (LTP) in both genotypes, the magnitude of LTP tended to be larger in GD slices (Fig. 8D, E).

Discussion

In this study, we generated the first knock-in mouse model in which N-cadherin is systemically replaced into an ADAM10-uncleavable form. In contrast to the previous reports of N-cadherin knock-out mice, showing severe systemic and neural anomalies [2,4,22], GD mutant mice grow and breed normally, but exhibit a set of unique phenotypes that include 1) enhanced fidelity (or reduced error rate) in a spatial working memory task, and 2) synapse anomaly (more distribution density, less PSD area) in the CA3 regions.

N-cadherin-mediated cell/synapse adhesion is augmented by the cytoplasmic anchorage to the actin cytoskeleton via p120/β/α-catenins and terminated by the proteolytic cleavages, which release extracellular and cytoplasmic fragments[23,24]. The relative stability of GD mutant N-cadherin on the cell surface (Fig. 2A, B) and the absence of the cytoplasmic fragment CTF1 (Fig. 3B) indicate augmentation of N-cadherin-based cell-cell adhesion in GD mice. Previous report by other group demonstrated that expression of a stable β-catenin mutant augments N-cadherin-mediated synaptic adhesion in vivo, without significantly affecting synaptic transmission and LTP [25,26]. Interestingly, in the mouse model, N-cadherin stabilization slows synapse remodeling and causes behavioral inflexibility in reversal learning and memory extinction, and drug addiction [25,26]. The phenotype of GD mice is concordant as to the normal synaptic transmission and LTP. Interestingly, behavioral change similar to 'inflexibility' in associative learning and memory was observed in GDmice, *i.e*, excessive freezing in the late phases of fear memory acquisition and of re-exposure to the context (Fig. 5A, B). Interestingly, in the cued testing in altered context on Day 2, mutants showed enhanced freezing even in the pre-CS period (Fig. 5A), indicating the occurrence of 'fear generalization'. This phenotype might be due to failure to eliminate previous fear memory when exposed to an altered context. Fear generalization has been attributed to hippocampal CA3 and dentate gyrus [27,28], thus, behavioral change observed in GD mice, i.e. better working memory and fear generalization, might be closely related to synapse anomaly in CA3 region of GD mice, observed in the present study.

Conditional knockout of ADAM10 in post-natal mouse brain perturbs N-cadherin cleavage, LTP, dendritic spine morphology (*i.e.*, reduced density, stubby shape), and causes seizure [29]. Pharmacological inhibition of ADAM10 results in spine enlargement *in vitro* and *in vivo* [30]. These cases contrast sharply with quasi-normal phenotype of GD mice with normal-sized dendritic spines (Fig. 6A). Given that ADAM10 cleaves not only N-cadherin, but also many other synaptic substrates that modulate spine shape and adhesion to the presynaptic counterparts [31], the phenotypic difference is attributed to the pleiotropy of ADAM10. On the other hand, spine enlargement caused by GD mutant expression (in addition to the endogenous N-cadherin) [30] may be interpreted as a phenotype caused by simple N-cadherin excess [13], because spine volume is demonstrated to be normal in GD mice, which express normal level of full-length N-cadherin (Fig. 3A).

Dendritic spine volume and PSD area, two principal morphometric indices that reflect the excitatory synapse activity, tightly correlate [32]. Intriguingly, however, CA3 regions of GD mice densely contain disproportionate synapses with small PSD area on normal-sized spines (Fig. 7B-D). The mechanism underlying this anomaly is unclear, but there are a few possibilities that are not mutually exclusive. 1)

Circuit immaturity: Synapses prematurely stabilized by excess N-cadherin may resist activity-dependent competitive elimination and pruning [33,34]. 2) Adaptive compensation (homeostatic scaling): Too many excitatory inputs into a given neuron may suppress maturation of individual synapses [35]. 3) Active zone confinement: N-cadherin excess may expand “non-active” synaptic contact around active zone [36]. Given that activity-dependent N-cadherin upregulation contributes to post-epileptic rewiring in CA3 region [37], similar disproportion and/or high-density synapse anomalies may constitute the pathology.

Conclusions

Overall, this study has provided *in vivo* evidence that ADAM10-mediated cleavage is a critical step in N-cadherin shedding and degradation at glutamatergic synapses, which alters hippocampal synapse morphology and animal behaviors related to spatial working memory and contextual fear memory. The unique mouse model established in this study will serve as a tool to explore the roles of N-cadherin processing in physiological synapse remodeling, and the pathological dysregulations which accompany epilepsy, Alzheimer’s disease, anxiety disorders and other neurological disorders.

Methods

Animal experiments

Animal experiments were approved by institutional review committees and conducted in accordance with the regulations for the care and use of animals at Kyoto University and Nippon Medical School. We compared male littermates raised in the same cages, unless otherwise noted.

Generation and establishment of a line of *Cdh2*$^{R714G, I715D}$ knock-in mice

We designed a targeting vector that spans a 9.6 kb region of the mouse the *Cdh2* gene to replace six bases in exon 13 from ^{6656}AGGATC to GGGGAT. After electroporation of the linearized vector into C57BL/6 mouse-derived Bruce 4 embryonic stem cells and selection of neomycin-resistant clones, we verified homologous recombination by Southern blotting and PCR (5’ side probes; Fw-GATGCTGCTAACAGATGACTACAGA, Rv-AAAGGTACTGACAATAGGGCTCATA and 3’ side probes; Fw-TCTCAAAGACTCCTATTGCTGTTCT, Rv-GTGTCTATAAGCTCCCATCAATGTC) of the genomic DNA. After blastocyst injection of the recombinant clones, we obtained chimera mice, which were crossbred with transgenic mice that ubiquitously express Cre-recombinase (*CAG-Cre*, C57BL/6, RBRC01828). Through backcrossing with C57BL/6J mice for more than two generations, we verified the removal of the neomycin-resistant gene cassette and the *CAG-Cre* allele by Southern blotting and PCR, and Mendelian transmission of the *Cdh2*$^{R714G, I715D}$ allele. We bred heterozyzous *Cdh2*$^{R714G, I715D/+}$ mice to generate homozygous (*Cdh2*$^{R714G, I715D/R714G, I715D}$; GD) and control (*Cdh2*$^{+/+}$; WT) littermates for experiments. The line has been deposited with the Center for Animal Resources and Development, Kumamoto University (ID 2027).

Genotyping

DNA from tail snips was purified using the automatic DNA isolation system PI-50(KURABO, Japan). Mouse *Cdh2* gene were amplified using the following primers: Forward = CCA CTT CTA AGC ATG CAG GT; Reverse = AAT GAC TCC TAT TTG AGC ACA

Behavioral analyses

We conducted behavioral tests with male littermates during 3–5 months of age, using an established protocol [38]. The behavioral tests were conducted in the following order: general health and neurological screening (including body weight and temperature measurements, grip strength test, and righting, whisker touch, and ear twitch reflexes), wire hang test, Barnes maze test, eight-arm radial maze test, and fear conditioning test.

Eight-arm radial maze test

The protocol was as previously described [39]. We used an apparatus with a central platform connected to eight arms (40-cm long with 25-cm high transparent walls, food pellet wells and sensors at distal ends) with automated shutters, which was placed 75 cm above the floor in a dim room with several spatial cues. The animals were starved for over a week to induce 15-20% weight loss and started on pre-training on the eighth day. We allowed a mouse to explore and eat food pellets for 30 min. Then, we set a pellet in a well and let a mouse explore and eat it, which was repeated eight times, once for each arm. In the spatial working memory task, we set a pellet in each well, and observed until a mouse ate the eight pellets. After each visit to an arm, the shutters were closed for 5 s with mice at the center. We video-monitored and analyzed arm choices, latency to acquire eight pellets, distance traveled, the number of times empty arms were chosen in the first eight choices, and the number of revisiting errors. Image RM software was used for the control of shutters, data acquisition and analysis (see below for 'IMAGE ANALYSIS').

Contextual and cued fear conditioning test

To assess fear memory [40], mice were placed in a conditioning chamber (26×34×29 cm) in a sound attenuated room and allowed to explore freely for 2 min. The animals were presented with an auditory cue (55 dB white noise) which served as a conditioned stimulus (CS) for 30 sec. During the last 2 sec of the CS, mice were given a mild foot shock (2 sec, 0.35 mA) as an unconditioned stimulus (US). Two more CS-US pairings were presented with 120 sec interval. 24 hrs later, context test was performed. Cued test in an altered context was performed using a triangular box (35×35×40 cm) made of white opaque plexiglas, located in a different room. Following initial 3-min of pre-CS period, the CS was presented for 3 min. Data acquisition, control of stimuli (white noise and foot shock), and data analysis were performed automatically using Image FZ software.

Image analysis

The application programs for behavioral data acquisition and analysis (Image BM, RM, FZ) were created on the platform of ImageJ (http://rsb.info.nih.gov/ij/) by TM.

Antibodies

We used commercial antibodies for the following antigens: N-cadherin (clone 32) and syntaxin-6 (clone 30, BD); β-actin, PSD95, and HA (Sigma); synaptophysin (clone SY38, Abcam); ADAM10 (AB19026), Presenillin1 (MAB5232), GluA1 (MAB2263), and GLT1 (MAB2262, Chemicon/Millipore); GluA2 (#13607), AKT (#9272), phospho-AKT (#9271), and α-Tubulin (#2144, CST); mouse and rabbit IgG, HRP-conjugated (NA931V and NA931934, GE Healthcare).

Plasmids

Ncad HA and NcadGD HA constructs, expressing the full-length human N-cadherin tagged with HA in C-terminus, as described elsewhere [20].

Primary mouse cortical neuron culture:

Primary neurons from GD mice brain were obtained from the cerebral cortices of fetal mice (14-16 days of gestation). Obtained cells were maintained in Neurobasal medium (Gibco) containing GlutaMAX™-I(Gibco), B-27 supplement (Gibco) and 1% penicillin/streptomycin (Nacalai tesque).

Immunofluorescence

Chinese Hamster Ovary (CHO) cells were maintained in Dulbecco's Modified Eagle Medium/Nutrient Mixture DMEM/F-12 (Thermo scientific) containing 10% FBS (Invitrogen) and 1% penicillin/streptomycin (Nacalai tesque). For transient expression, Lepofectamin2000^{TM} (Invitorogen), was used. After 24hrs, CHO were fixed, permeabilized and incubated in Block Aid (Thermo) for 1 hr. The primary antibodies against HA (1:1000) and β-catenin (1:1000) were incubated at 4 ℃ overnight. The secondary antibodies conjugated to Alexa-Fluor 488/546 were added for 1 h at room temperature. Cells were mounted onto slides by ProLong Gold antifade reagent with DAPI (Molecular Probes). Images were acquired using FLUOVIEW FV10i (OLYMPUS).

Internalization assay

CHO cells were transfected with Ncad-HA(WT) or Ncad GD-HA(GD mutant) and incubated with 1mg/ml Sulfo-NHS-LC-Biotin(Thermo) in KRPH Buffer(128mM NaCl, 4.7mM KCl, 1.25mM $CaCl_2$, 1.25mM $MgSO_4$, 5mM NaH_2PO_4, 20mM HEPES) at 4℃ for 1hr. Surface-biotinylated cells were washed in PBS and washed twice more with Biotin Blocking Reagent (50mM NH_4Cl, 1mM $MgCl_2$, 0.1mM$CaCl_2$). Cells were replaced in DMEM/F12 containing 10% FBS and incubated at 37℃ for 1,3,6,12 hr. After incubation, cells were lysed in RIPA buffer (20mM Tris-HCl pH7.4, 150 mM NaCl, 0.1% SDS, 1% TritonX-100, 1% Sodium Deoxycholate,

5mM EDTA containing a protease inhibitor mix). Surface-biotinylated proteins were pulled down with streptavidin beads (Invitrogen), subjected to SDS PAGE and blotted with anti-HA-tag antibody (Sigma).

Preparation of synaptosome

Synaptosome was prepared according to the previous report of P.R. DODD et al [41]. In brief, mouse brain tissue was homogenized in 10 volumes of homogenization buffer (5 mM HEPES buffer, pH 7.4, containing 0.32 M sucrose, 50 mM sodium fluoride, with phosphatase and protease inhibitor cocktail) in a Potter–Elvehjem homogenizer. The homogenate was centrifuged at 1000 *g* at 4°C for 5 min, twice. Supernatant was layered directly onto 1ml 1.2 M sucrose and centrifuged at 50,000 rpm at 4℃ for 10 min. The Pellet of intermediate layer was collected and diluted with ice-cold 0.32 M sucrose to a final volume of 1 ml. The diluted suspension was then layered onto 0.8 ml of 0.8 M sucrose and centrifuged once again at 50,000 rpm at 4°C for 15 min. The pellet was suspended in RIPA buffer (with protease and phosphatase inhibitors. The pellet was then layered over discontinuous sucrose gradient (0.85–1.0–1.2 *M*) and centrifuged at 85,000*g* for 2h at 4°C. Synaptosomal fraction was obtained at the interface of 1 and 1.2 M sucrose.

Immunoblotting

Immunoblotting was analyzed as previously described [42].

Golgi Staining

Golgi staining was performed using a Rapid GolgiStain kit according to the manufacturer's protocol (FD NeuroTechnologies, Columbia,MD). Mice were sacrificed at the age of 4 months. The brains were immersed in impregnation solution for 2 weeks in the dark, and then stored at 4℃ for a week. The brain samples were dipped into isopentane pre-cooled with dry ice, mounted with TFM (TBS,Durham,Nc,USA), sliced (80μm) with a cryostat ,and then mounted on gelatin-coated glass slides. Subsequently, the sections were stained with staining solution. Measurements of the spine area were made by Image J and Metamorph (Molecular Devices).

Serial section transmission electron microscopy (ssTEM)

See reference [43].

Electrophysiology

Mice were decapitated under deep halothane anesthesia at the age of 14 to 15 weeks, and both hippocampi were isolated. Transverse hippocampal slices (380 μm) were cut using a tissue slicer and maintained in a humidified interface holding chamber. Electro-physiological recordings were performed as described [44]. Recordings were made in a submersion-type chamber maintained at 27.0 - 27.5 ºC and superfused at 2 ml/min with saline composed of (in mM): NaCl, 125; KCl, 2.5; NaH_2PO_4, 1.0; $NaHCO_3$, 26.2; glucose, 11; $CaCl_2$, 2.5; $MgCl_2$, 1.3. For recording EPSPs arising from the A/C fiber-pyramidal cell

synapses, a glass recording pipette filled with 2 M NaCl and bipolar stimulating electrodes were placed in the stratum radiatum of the CA3 region. The initial slope of EPSPs was measured on analysis. Single electrical stimulation was delivered at a frequency of 0.05 Hz, unless otherwise specified. To induce LTP, high-frequency burst stimulation (5 pulse at 100 Hz, repeated 10 times at 5 Hz) was delivered 3 times at an interval of 20 s. All recordings were made using a Multiclamp 700B amplifier (Molecular Devices, Sunnyvale, CA, USA).

Statistical analysis

Quantitative data were expressed as mean ± SEM. For statistical analyses, either two tailed t-test or ANOVA (one-way, two-way repeated measures, and repeated measures with two factors) was applied using StatView (SAS institute). F and p values represent the effects of genotype, unless otherwise noted.

Abbreviations

NMDAR
N-Methyl-D-Aspartate receptor; ADAM10:A-disintegrin and metalloprotease 10; PSD:Postsynaptic density; AMPA:α-3-hydroxy-5-methyl-4-isoxazole propionic acid; HA:Human influenza hemagglutinin; CHO:Chinese hamster ovary; ANOVA, analysis of variance; cx:cerebral cortex; KI:knock-in; wt:wild-type.

Declarations

Ethics approval and consent to participate

Recombinant DNA experiments and animal experiments were approved by Kyoto University Recombinant DNA Committee (180172) and Kyoto University Animal Experimentation Committee (MedKyo20014), respectively, and conducted in accordance with the regulations for the care and use of animals at Kyoto University and Nippon Medical School.

Consent for publication

All authors consent to publication of this manuscript as a research article.

Competing interests

The authors declare that they have no competing interests.

Authors contributions

KU and AK designed and supervised the establishment of the mouse line at Unitech Co. Ltd. MA-U conducted the biochemical and cell biological analyses. MA-U, YN, YT and MK conducted animal experiments. KK conducted electrophysiological analyses, HY participated synaptosomal fractionation, MU-T analyzed the tufts of thorny excrescence, SH and TM analyzed behavioral test results, NA-I

conducted the EM analysis under the supervision of MK. MK and AK wrote the manuscript. MU and RT gave a critical advice throughout the experiments. All authors read and approved the manuscript.

Funding

AK was supported by Health Labour Sciences Research Grant from the Ministry of Health Labour and Welfare (H17-Choju-005) and Grant-in-Aid for Scientific Research(B) (20300124) from Ministry of Education, Culture, Sports, Science and Technology in Japan. This study is partly supported by "Joint Usage/Research Center for Genes, Brain and Behavior “accredited by Minister of Education, Culture, Sports, Science and Technology in Japan (for authors of Fujita Medical School).

Availabilities of data and materials

Data sharing not applicable to this article as no datasets were generated.

Acknowledgements

We thank Dr. Y Hatanaka for the spine morphology analysis, Y. Mano (Nagoya University) for technical assistance, and H. Nakabayashi for formatting figures.

References

1. Dalva MB, McClelland AC, Kayser MS. Cell adhesion molecules: signalling functions at thesynapse. Nat Rev Neurosci. 2007; (8), 206–220.
2. Kadowaki M, Nakamura S, Machon O, Krauss S, Radice GL, Takeichi M. N-cadherinmediates cortical organization in the mouse brain. Dev Biol. 2007;304:22–33.
3. Arikkath J, Reichardt LF. Cadherins and catenins at synapses: roles in synaptogenesis and.
4. synaptic plasticity. Trends Neurosci. 2008;31:487–94.
5. Hirano S, Takeichi M. Cadherins in brain morphogenesis and wiring. Physiol Rev. 2012;92:597-.
6. 634.
7. 5. Nikitczuk JS, Patil SB, Matikainen-Ankney BA, Scarpa J, Shapiro ML, Benson DL,Huntley GW. N-cadherin regulates molecular organization of excitatory and inhibitory synaptic circuits in adult hippocampus in vivo. Hippocampus.2014; 24, 943–962.
8. 6. Chazeau A, Garcia M, Czöndör K, Perrais D, Tessier B, Giannone G, Thoumine O. Mechanical coupling between transsynaptic N-cadherin adhesions and actin flow stabilizes dendritic spines. Mol Biol Cell. 2015; 26, 859–873.
9. 7. Uchida N, Honjo Y, Johnson KR, Wheelock MJ, Takeichi M. The catenin/cadherin adhesion system is localized in synaptic junctions bordering transmitter release zones. J Cell Biol. 1996; 135, 767–779.

10. 8. Tanaka H, Shan W, Phillips GR, Arndt K, Bozdagi O, Shapiro L, Huntley GW, Benson DL, Colman DR. Molecular modification of N-cadherin in response to synaptic activity.Neuron. 2000; 25, 93–107.
11. 9. Togashi H, Abe K, Mizoguchi A, Takaoka K, Chisaka O, Takeichi M. Cadherin regulates
12. dendritic spine morphogenesis. Neuron.2002; 35, 77–89.
13. 10. Abe K, Takeichi M. NMDA-receptor activation induces calpain-mediated beta-catenin
14. cleavages for triggering gene expression. Neuron.2007; 53, 387–397.
15. 11. Tai CY, Mysore SP, Chiu C, Schuman EM. Activity-regulated N-cadherin endocytosis.
16. Neuron.2007; 54, 771–785.
17. 12. Bozdagi O, Wang XB, Nikitczuk JS, Anderson TR, Bloss EB, Radice GL, Zhou Q, Benson
18. DL, Huntley GW. Persistence of coordinated long-term potentiation and dendritic spine
19. enlargement at mature hippocampal CA1 synapses requires N-cadherin. J Neurosci.2010;30:9984–9989.
20. 13. Mendez P, De Roo M, Poglia L, Klauser P, Muller D. N-cadherin mediates plasticity-
21. induced long-term spine stabilization. J. Cell Biol.2010; 189:589–600.
22. 14. Uemura K, Kihara T, Kuzuya A, Okawa K, Nishimoto T, Bito H, Ninomiya H, Sugimoto H, Kinoshita A, Shimohama S. Activity-dependent regulation of beta-catenin via epsilon-cleavage of N-cadherin. Biochem Biophys Res Commun. 2006; 345(3):951-8.
23. 15. Restituito S, Khatri L, Ninan I, Mathews PM, Liu X, Weinberg RJ, Ziff EB. Synaptic
24. autoregulation by metalloproteases and γ-secretase. J Neurosci.2011; 31, 12083–12093.
25. 16. Shinoe T, Goda Y. Tuning synapses by proteolytic remodeling of the adhesive surface.Curr
26. Opin Neurobiol.2015; 35:148–155.
27. 17. Fortini, M. E. Gamma-secretase-mediated proteolysis in cell-surface- receptor signalling.
28. Nat. Rev. Mol. Cell Biol. 2002; 3, 673–684.
29. 18. Marambaud, P., Wen, P. H., Dutt, A., Shioi, J., Takashima, A., Siman, R. and Robakis,N. K. A CBP binding transcriptional repressor produced by the PS1/epsilon-cleavage of N-cadherin is inhibited by PS1 FAD mutations. Cell.2003; 114, 635–645.
30. 19. Reiss K, Maretzky T, Ludwing A, Tousseyn, De Strooper B, Hartmann D, Saftig P.
31. ADAM10 cleavage ofN-cadherin andregulation ofcell-cell adhesion and beta-catenin nuclear signalling. EMBO J. 2005; 24(4), 742 – 52.
32. 20. Uemura K, Kihara T, Kuzuya A, Okawa K, Nishimoto T, Ninomiya H, Sugimoto H, Kinoshita A, Shimohama S. Characterization of sequential N-cadherin cleavage by ADAM10 and PS1.Neurosci Lett. 2006; 24;402(3):278 – 83.
33. 21. Reiss K, Maretzky T, Ludwig A, Tousseyn T, de Strooper B, Hartmann D, Saftig P.
34. ADAM10 cleavage of N-cadherin and regulation of cell-cell adhesion and beta-catenin
35. nuclear signalling.EMBO J.2005.

36. 22. Radice GL, Rayburn H, Matsunami H, Knudsen KA, Takeichi M, Hynes RO. Developmental defects in mouse embryos lacking N-cadherin. Dev Biol. 1997;181, 64–78.
37. 23. Brigidi GS, Bamji SX. Cadherin-catenin adhesion complexes at the synapse. Curr Opin
38. Neurobiol. 2011; 21, 208–214.
39. 24. Benson DL, Huntley GW. Synapse adhesion: a dynamic equilibrium conferring stability and
40. flexibility. Curr Opin Neurobiol.2012; 22(3):397–404.
41. 25. Mills F, Bartlett TE, Dissing-Olesen L, Wisniewska MB, Kuznicki J, Macvicar BA,Wang YT, Bamji SX. Cognitive flexibility and long-term depression (LTD) are impaired following β-catenin stabilization in vivo. Proc Natl Acad Sci U S A. 2014; 111, 8631–8636.
42. 26. Mills F, Globa AK, Liu S, Cowan CM, Mobasser M, Phillips AG, Borgland SL, Bamji SX. Cadherins mediate cocaine-induced synaptic plasticity and behavioral conditioning.Nat Neurosci. 2017; 20, 540–549.
43. 27. Cravens CJ, Vargas-Pinto N, Christian KM, Nakazawa K. CA3 NMDA receptors are crucial for rapid and automatic representation of context memory. Eur J Neurosci. 2006; 24:1771–1780.
44. 28. McHugh TJ, Jones MW, Quinn JJ, Balthasar N, Coppari R, Elmquist JK, Lowell BB, Fanselow MS, Wilson MA, Tonegawa S. Dentate gyrus NMDA receptors mediate rapid pattern separation in the hippocampal network. Science. 2007; 317: 94–99.
45. 29. Prox J, Bernreuther C, Altmeppen H, Grendel J, Glatzel M, D'Hooge R, Stroobants S, Ahmed T, Balschun D, Willem M, Lammich S, Isbrandt D, Schweizer M, Horré K, De Strooper B, Saftig P. Postnatal disruption of the disintegrin/metalloproteinase ADAM10 in brain causes epileptic seizures, learning deficits, altered spine morphology, and defective synaptic functions. J Neurosci. 2013; 33, 12915–12928.
46. 30. Malinverno M, Carta M, Epis R, Marcello E, Verpelli C, Cattabeni F, Sala C, Mulle C, Di Luca M, Gardoni F. Synaptic localization and activity of ADAM10 regulate excitatory synapses through N-cadherin cleavage. J Neurosci. 2010; 30(48):16343-55.
47. 31. Kuhn PH, Colombo AV, Schusser B, Dreymueller D, Wetzel S, Schepers U, Herber J,Ludwig A, Kremmer E, Montag D, Müller U, Schweizer M, Saftig P, Bräse S, Lichtenthaler SF. Systematic substrate identification indicates a central role for the metalloprotease ADAM10 in axon targeting and synapse function. Elife.2016; 5, e12748.
48. 32. Arellano JI, Benavides-Piccione R, Defelipe J, Yuste R. Ultrastructure of dendritic spines:
49. correlation between synaptic and spine morphologies. Front Neurosci.2007; 1, 131–143.
50. 33. Elste AM, Benson DL. Structural basis for developmentally regulated changes in cadherin
51. function at synapses. J Comp Neurol.2006; 495, 324–335.
52. 34. Bian WJ, Miao WY, He SJ, Qiu Z, Yu X. Coordinated spine pruning and maturation mediated by inter-spine competition for cadherin/catenin complexes. Cell.2015; 162,808–822.
53. 35. Peng YR, He S, Marie H, Zeng SY, Ma J, Tan ZJ, Lee SY, Malenka RC, Yu X. Coordinated
54. changes in dendritic arborization and synaptic strength during neural circuit development.

55. Neuron.2009; 61, 71–84.
56. 36. Ageta-Ishihara N, Konno K, Yamazaki M, Abe M, Sakimura K, Watanabe M, Kinoshita M.
57. CDC42EP4, a perisynaptic scaffold protein in Bergmann glia, is required for glutamatergic
58. tripartite synapse configuration. Neurochemistry International.2018; 119, 190–198.
59. 37. Shan W, Yoshida M, Wu XR, Huntley GW, Colman DR. Neural (N-) cadherin, a synaptic adhesion molecule, is induced in hippocampal mossy fiber axonal sprouts by seizure.J Neurosci Res.2002; 69, 292–304.
60. 38. Takao K, Yamasaki N, Miyakawa T. Impact of brain-behavior phenotypying of genetically-engineered mice on research of neuropsychiatric disorders. Neurosci Res. 2007; 58,124–132.
61. 39. Koshimizu, H., Y. Fukui, K. Takao, K. Ohira, K. Tanda, K. Nakanishi, K. Toyama,M.
62. Oshima, M. M. Taketo, and T. Miyakawa. Adenomatous polyposis coli heterozygous
63. knockout mice display hypoactivity and age-dependent working memory deficits: Front
64. Behav Neurosci, 2011.
65. 40. Shoji H, Takao K, Hattori S, Miyakawa T. Contextual and cued fear conditioning test using
66. a video analyzing system in mice. J Vis Exp. 2014.
67. 41. P.R.DODD, J.A.HARDY, A.E.OKLEY, J.A. EDWQRDSON, E.K. PERRY and J.P.DELAUNOY. A rapid method for preparing syanptosomes; Comparison, with alternative procedures. Brain.Res.1981;226.
68. 42. Megumi Asada-Utsugi, Kengo Uemura, Akira Kuzuya, Masato Maesako, Koichi Ando, Masakazu Kubota, Kiwamu Watanabe, Makio Takahashi, Takeshi Kihara, Shun Shimohama, Ryosuke Takahashi, Oksana Berezovska and Ayae Kinoshita. N-cadherin enhances APP dimerization at the extracellular domain and modulates Aβ production. J Neurochem. 2011; 119(2):354 – 63.
69. 43. L K Parafuli, N Ageta-Ishihara, H Ageta, Y Fukazawa, M Kinoshita. Chapter 16 -Methods for immunoblot detection and electron microscopic localization of septin subunits in mammalian nervous systems. Methods in Cell Biology.2016; 136, 285–294.
70. 44. Kobayashi K, Suzuki H. Dopamine selectively potentiates hippocampal mossy fiber to CA3 synaptic transmission. Neuropharmacology.2007; 52, 552–561.

Figures

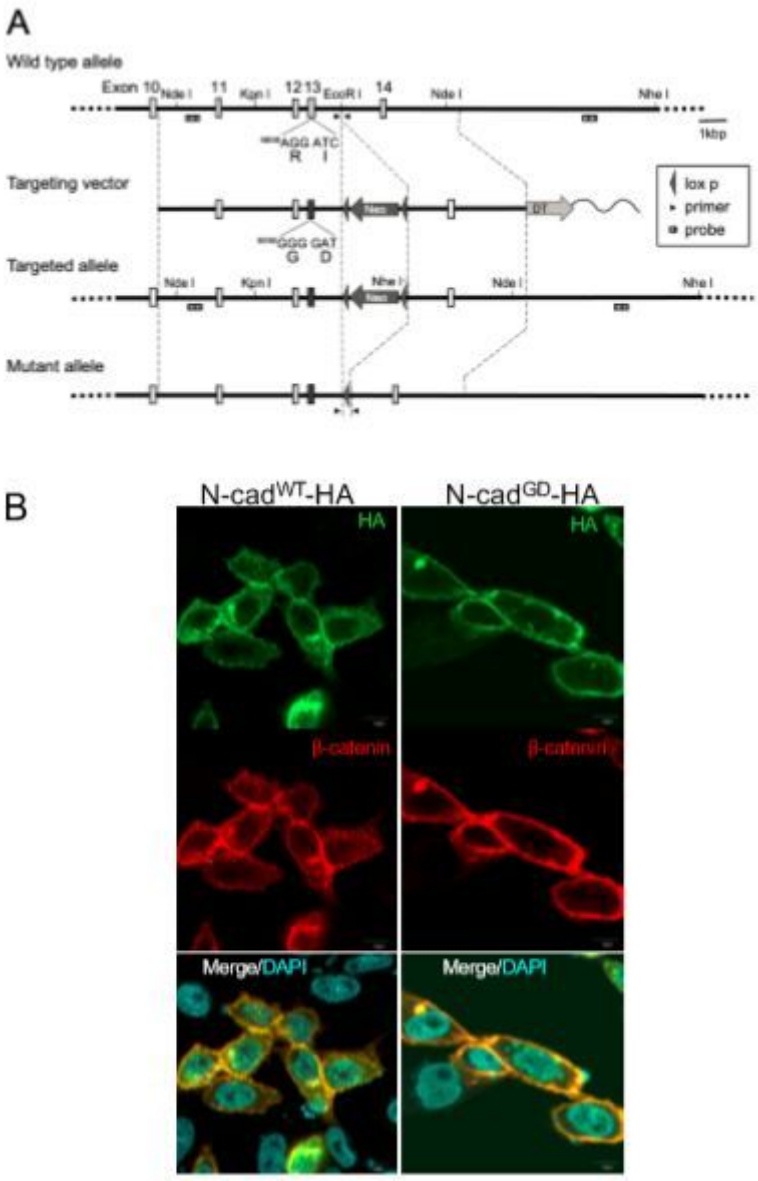

Figure 1

Introducing ADAM10-uncleavable GD mutations into N-cadherin/Cdh2 in the mouse genome, and testing the mutant distribution in cultured cells (A) Genomic DNA map of the mouse Cdh2 gene locus, mutant design, and targeting strategy. The gene targeting vector was designed to introduce tandem missense mutations (6656AGG ATC for 714RI → GGG GAT for GD) in the exon 13 of the mouse Cdh2 gene. The targeting vector was introduced into C57BL/6-derived ES cells by electroporation. Neomycin-resistant clones were screened for homologous recombination with genomic Southern blotting using two probes, and one such clone was injected into ICR blastocysts. The resulting chimera mice were intercrossed with C57BL/6N mice. The floxed neomycin-resistant cassette was removed from the allele by intercrossing the F1 mice with a line of CAG-Cre driver mice of C57BL/6 strain. The mutant and wild type alleles were discriminated routinely by PCR genotyping, using a pair of primers (arrowheads). See Materials and Methods for details. (B) Representative immunofluorescence images of FLAG-tagged, WT and GD mutant N-cadherin expressed in CHO cells. Their distribution patterns on ER, Golgi apparatus, and plasma

membrane (green), as well as colocalization with endogenous β-catenin (red), were comparable. Nuclear DNA is stained with DAPI (cyan).

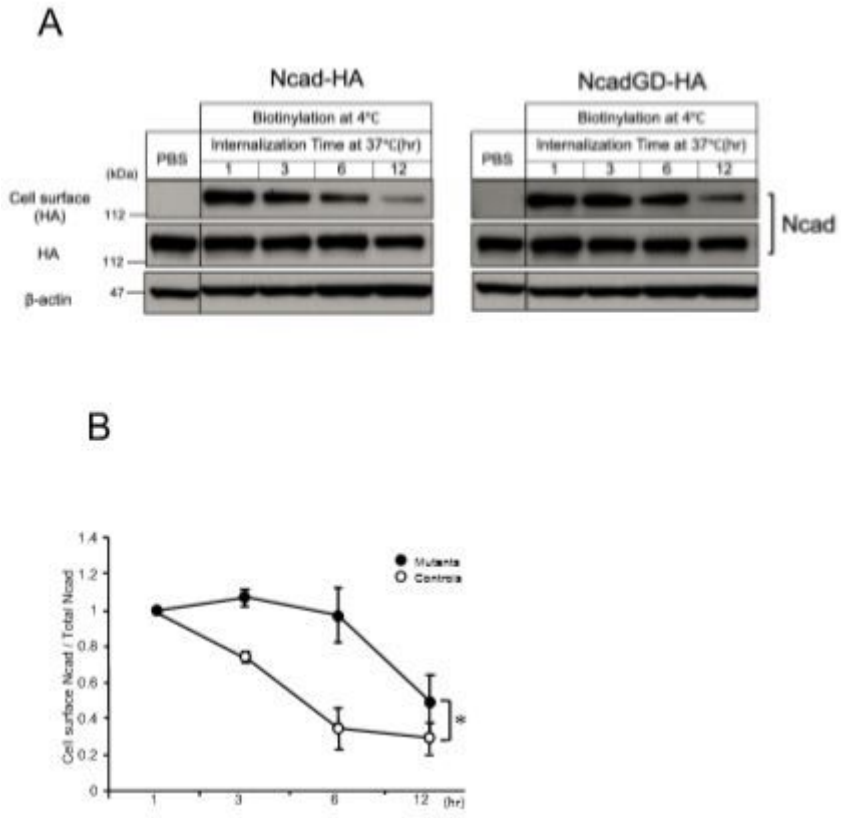

Figure 2

GD mutant N-cadherin on the plasma membrane is relatively stable (A) Representative immunoblot data from cell surface protein bio-tinylation analysis for HA-tagged, WT (left) or GD mutant (right) N-cadherin expressed in CHO cells. Surface bio-tinylation pulse-labeling followed by serial immunoblot assay for the HA epitope shows that cell surface fraction of GD and WT N-cadherins decay within hours, while the levels of total N-cadherins remain unchanged. Note that the cell surface fraction of GD N-cadherin was significantly more stable than that of WT. (B) (Top) Densitometric quantification of surface bio-tinylation assay demonstrated that GD mutant (●) on the plasma membrane decayed significantly more slowly than WT (●). (n=3, 3, p=0.0241, ANOVA)

Fig. 3

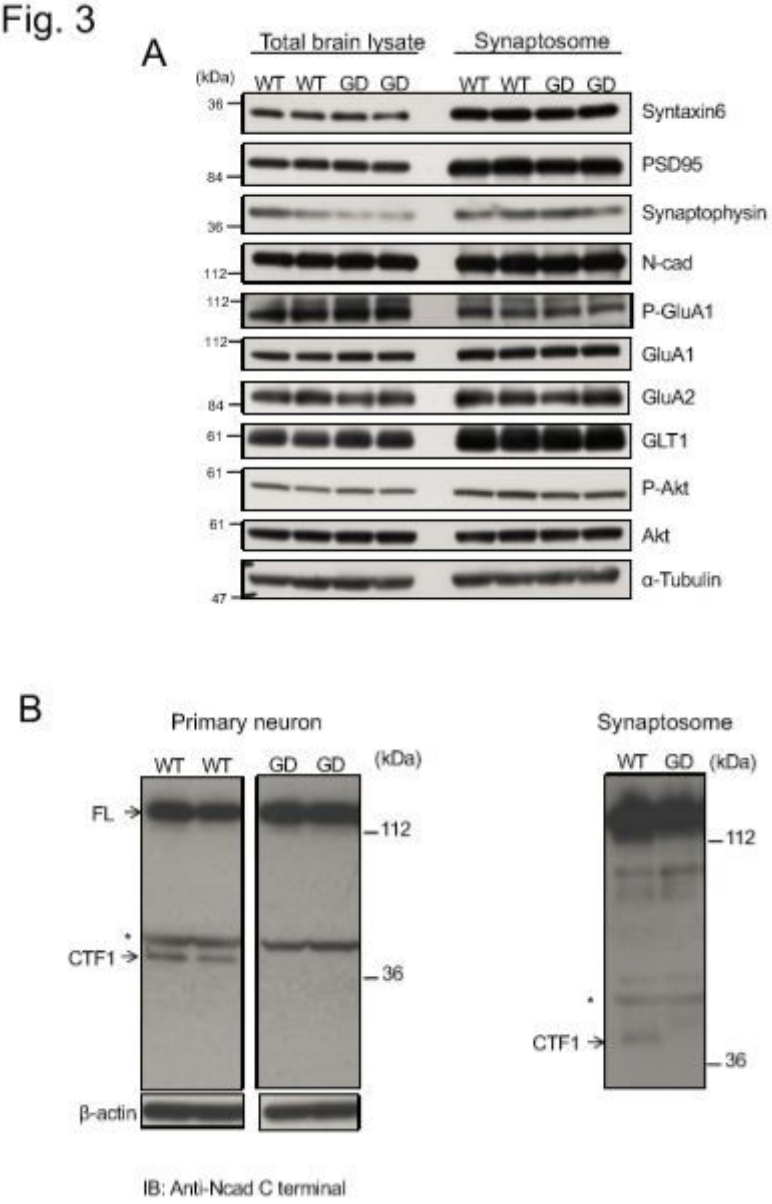

Figure 3

Protein profiles of GD mouse brain is normal but for the absence of CTF1 (A) Representative immunoblot of endogenous proteins related to glutamatergic synapse and/or N-cadherin in the total brain lysate and a synaptosomal fraction from GD and WT mice. No recognizable difference was found in syntaxin 6, PSD95, synaptophysin, full-length N-cadherin, phospho-GluA1, GluA1, GluA2, GLT-1, phospho-AKT, AKT, α-tubulin). (B) Immunoblot detection of endogenous N-cadherin with an antibody against a C-terminal region in the total lysates of primary cultured cerebrocortical neurons from WT and GD mice. While the full-length form (FL, 130kDa) was detected both in WT and GD samples, the cytoplasmic fragment CTF1 (45kDa) was detected only in those from WT, but not in those from GD mice (left). Similar results were obtained from the synaptosomal fraction (right). Non-specific bands appeared around 50kDa (*) and above.

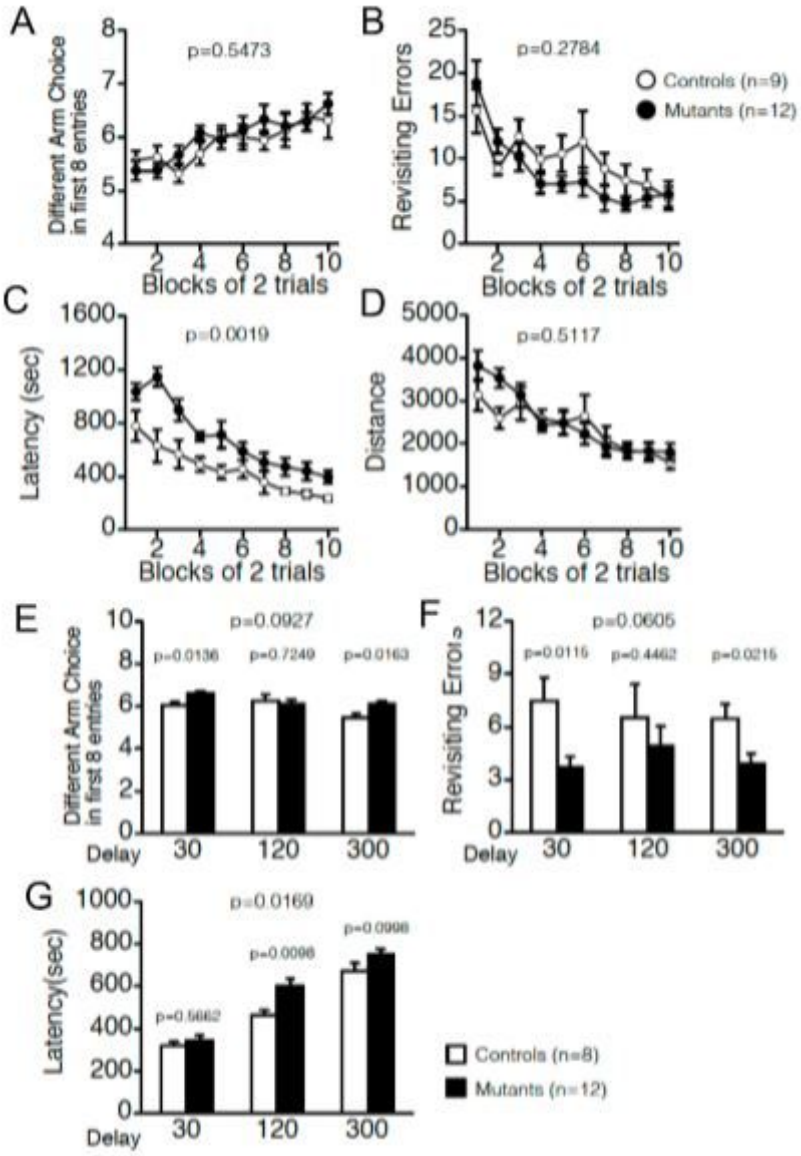

Figure 4

Improvement of working memory performance of GD mice in the eight-arm radial maze test. Spatial learning was tested in the eight-arm radial maze test on 4 months WT (□; n=9) and GD (■; n=12) mice. (A)The number of different arm choices in the first eight entries, (B) the number of revisiting errors, (C) the latency to acquire eight pellets and (D) and the distance traveled are presented. (E-G) Results of the eight-arm radial maze test with delays of 3, 120, 300 sec. The number of different arm choices in the first eight entries (E), the number of revisiting errors (F) and latency (G) were presented. One WT mouse died after trials. Values are means ± SEM.

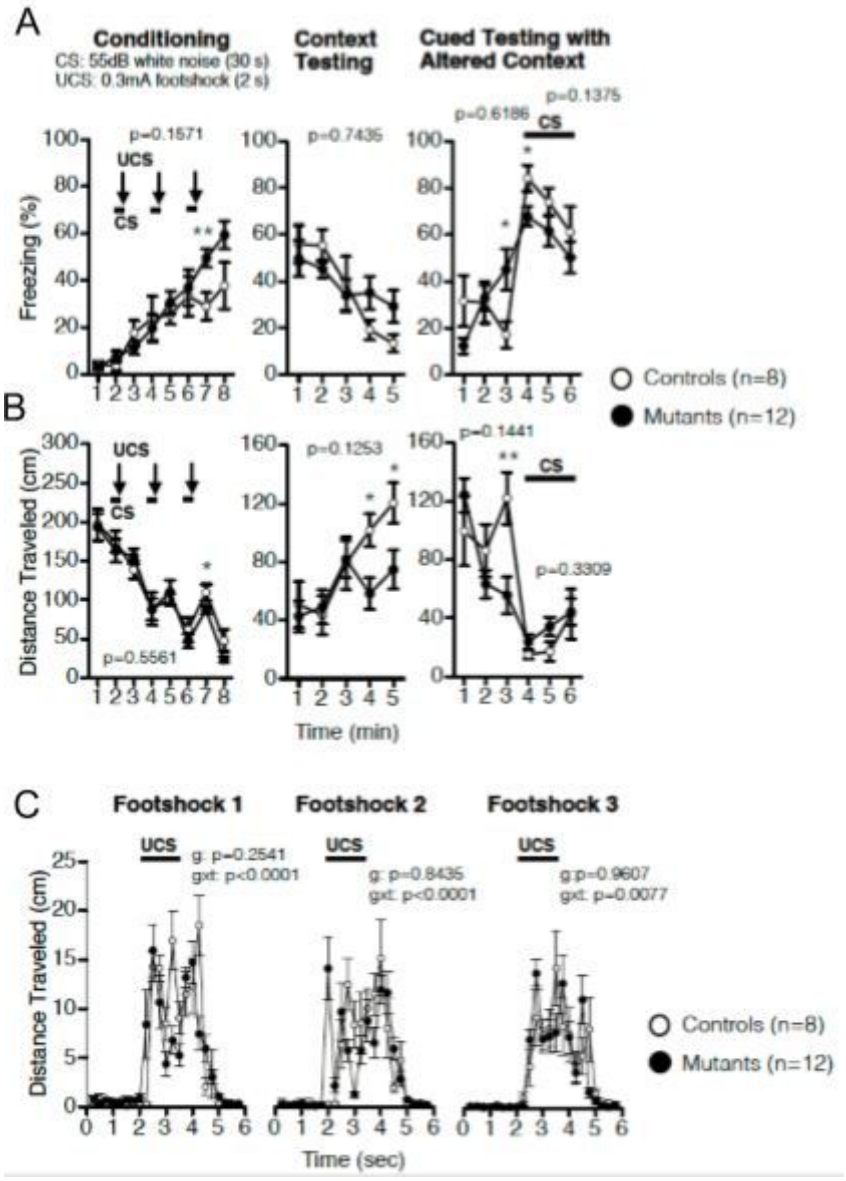

Figure 5

Fear conditioning test in GD mice. (A) Freezing (%) in the conditioning (left panel), context test (middle panel), and cued test (right panel). (B) Distance traveled (cm) in the conditioning (left panel), context test (middle panel), and cued test (right panel). (C) Distance traveled immediately after foot-shocks in the conditioning phase. Values are means ± SEM. WT □; n=8, GD ■; n=12.

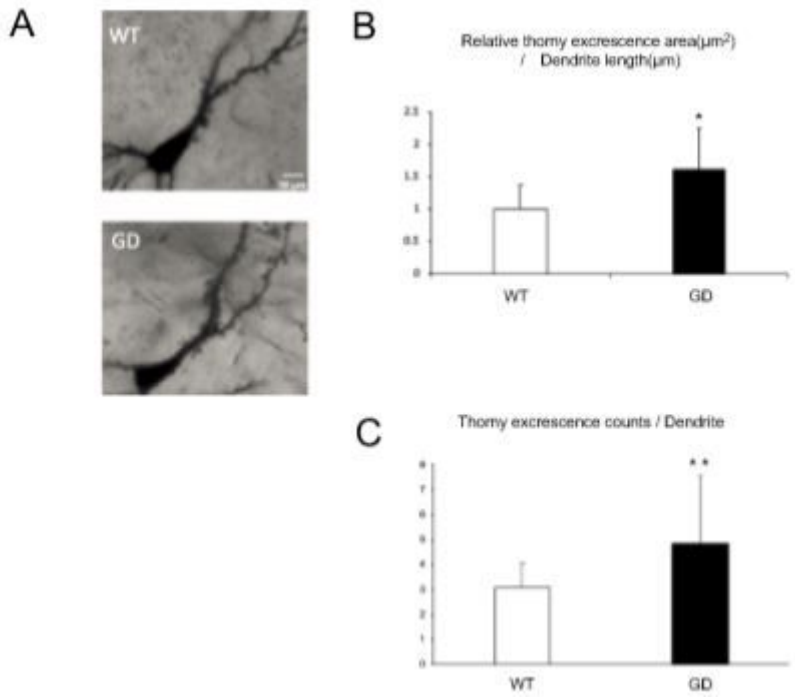

Figure 6

GD mice exhibit synapse anomalies in CA3 (A) Bright field micrographs of Golgi stained brain slices from the stratum lucidum of the CA3 region of the hippocampus. Note the complexity in the tufts of thorny excrescence. (B)The graph shows that the area of thorny excrescence per unit length of dendrite is significantly higher in GD mice. WT; n=12, GD; n=15, * p=0.0063, ANOVA. (C)Thorny excrescence counts per dendrite. ** p=0.0019, t-test.

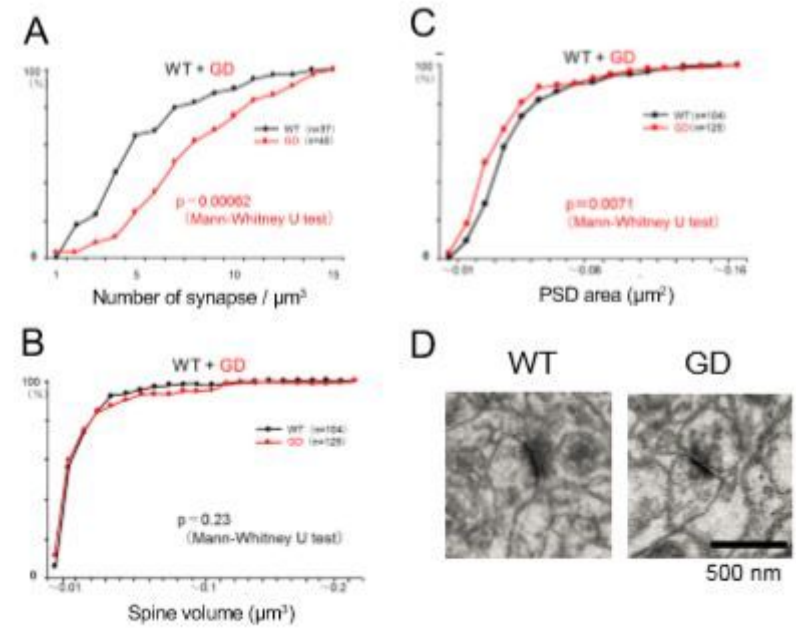

Figure 7

GD mice exhibit synapse anomalies in CA3 (A) Cumulative histogram of asymmetrical synapse density in the stratum radiatum of the CA3 region of the hippocampus. Synapse density measured by the dissector method was significantly higher in GD mice (median value, 7 vs. 4, n= 37, 40, p=0.00062, Mann-Whitney U-test). (B) Cumulative histogram of dendritic spine volume of asymmetrical synapses in the same region. Dendritic spine volume measured with ssTEM/3D reconstruction method was comparable between GD and WT mice (median value, 0.015 vs. 0.015, n= 104, 125, p=0.23, Mann-Whitney U-test). (C) Cumulative histogram of PSD area of asymmetrical synapses in the same region. PSD area measured with ssTEM/3D reconstruction method was significantly smaller in GD mice (median value, 0.030 vs. 0.035, n= 104, 125, p=0.0071, Mann-Whitney U-test). (D) Representative images of asymmetrical synapses at CA3 region observed by electron microscopy.

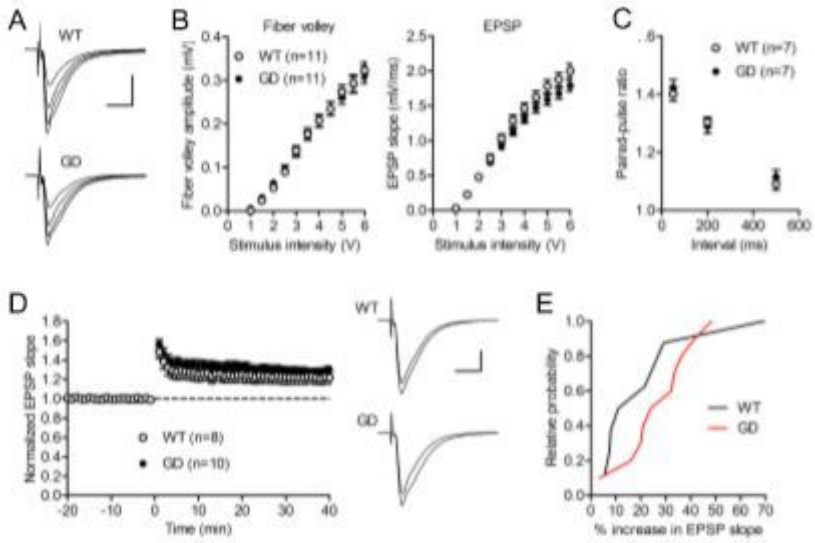

Figure 8

Marginal anomalies of A/C fiber-pyramidal cell synaptic transmission in CA3 (A) A/C fiber-pyramidal cell synaptic potentials evoked at the stimulus intensities of 2, 3, 4 and 5 V in WT and GD mice. Scale bar: 10 ms, 1 mV. (B) Dependence of fiber volley amplitude (left) and EPSP slope (right) on stimulus intensity. Statistically significant interaction between EPSP slopes and stimulus intensities was observed (two-way repeated measure ANOVA: $F_{10,200} = 3.2$, $p = 0.0008$). (C) Normal paired-pulse facilitation of EPSP slopes. (D) Mild augmentation of LTP in the mutant mice. High-frequency stimulation (HFS) was delivered at time 0. Sample traces are averages of 30 consecutive EPSPs during baseline and 30 to 40 min after HFS. (E) Cumulative relative probability distributions of the magnitude of LTP measured at 30 to 40 min after HFS. The number (n) of data represents the number of slices in this figure.